bioRxiv preprint doi: https://doi.org/10.1101/559104; this version posted February 24, 2019. The copyright holder for this preprint (which was not certified by peer review) is the author/funder. All rights reserved. No reuse allowed without permission.

Title: Persistence of neuronal representations through time and damage in the hippocampus.

Authors: Walter G. Gonzalez, Hanwen Zhang, Anna Harutyunyan, and Carlos Lois*

Affiliations:
[1] Division of Biology and Biological Engineering, California Institute of Technology, Pasadena, United States.

*Correspondence to: clois@caltech.edu.

Abstract:

Memories can persist for decades but how they are stably encoded in individual and groups of neurons is not known. To investigate how a familiar environment is encoded in CA1 neurons over time we implanted bilateral microendoscopes in transgenic mice to image the activity of pyramidal neurons in the hippocampus over weeks. Most of the neurons (90 %) are active every day, however, the response of neurons to specific cues changes across days. Approximately 40 % of place and time cells lose fields between two days; however, on timescales longer than two days the neuronal pattern changes at a rate of 1 % for each additional day. Despite continuous changes, field responses are more resilient, with place/time cells recovering their fields after a 10-day period of no task or following CA1 damage. Recovery of these neuronal patterns is characterized by transient changes in firing fields which ultimately converge to the original representation. Unlike individual neurons, groups of neurons with inter and intrahemispheric synchronous activity form stable place and time fields across days. Neurons whose activity was synchronous with a large group of neurons were more likely to preserve their responses to place or time across multiple days. These results support the view that although task-relevant information stored in individual neurons is relatively labile, it can persist in networks of neurons with synchronized activity spanning both hemispheres.

One Sentence Summary:

Neuronal representations in networks of neurons with synchronized activity are stable over weeks, even after lack of training or following damage.

bioRxiv preprint doi: https://doi.org/10.1101/559104; this version posted February 24, 2019. The copyright holder for this preprint (which was not certified by peer review) is the author/funder. All rights reserved. No reuse allowed without permission.

Main Text:

Memories are processed and stored by a complex network of neurons across several circuits in the brain; however, little is known about how information is encoded and retained in these neurons for long periods of time. Information could be stored at different hierarchical levels, within individual neurons through modification of their synapses, or distributed among many neurons in different brain areas including the hippocampus and cortex. The hippocampus is known to play an essential role in the formation of memories (*1*, *2*) and neurons in this brain area show robust response to space (place cells), time (time cells), or other task relevant cues (*3–5*). Many works have studied how neuronal activity in the hippocampus changes during learning (*6*, *7*), attention (*8*, *9*), and re-exposure (*10*). However, what aspects of neuronal activity in the hippocampus persist during future visits to a familiar environment, how is information encoded in group of neurons, and how lesions perturb the long-term maintenance of these neuronal patterns remains poorly understood.

The question of how information is stably encoded in neurons in the hippocampus remains a controversial issue. Whereas extracellular recordings show that place cells retain their fields from days to a weeks (*11*), calcium imaging experiments show drastic changes of neuronal activity across days (*12–15*). In freely moving mice place field were also observed to be the same across weeks but head-fixed preparation show drastic changes between days (*12–14*). Considering that the hippocampus is necessary for the formation, but not for the long-term maintenance of memories, it is possible that neuronal representations in the hippocampus may change over time as information is transferred from other brain areas (*16*). Previous long-term imaging of neuronal activity have shown that a large number of pyramidal neurons in CA1 are active during a 35 day period but only 31 % were active in each session and only 2.8 ± 0.3% were active in all sessions (*12*). However, the inability to detect active neurons on consecutive days could be due to motion artifacts caused by the removal and reattachment of the microendoscope between days. In addition, overexpression of GCaMP using AAVs can induce cell toxicity or even death (*17*). To overcome these potential limitations we built custom microendoscopes that were chronically implanted and performed long-term simultaneous bilateral imaging of hippocampal activity in freely moving Thy1-GCaMP6s mice **(Figure 1a, S1, and see supplementary data)** (*18–21*). The combination of chronic implants, high sensitivity microendoscope, improved cell detection and registration with the CNMFe software allowed us to minimize motion artifacts and to increase the reliability of long-term recordings **(Fig. 1b-c and S2)**(*22*, *23*). We imaged CA1 pyramidal neuron activity for several weeks through three situations, which we defined as follows: (i) "learning", during the initial 5 sessions of exposure to a novel linear track with sugar water reward at the ends, (ii) "re-exposure", after a 10-day period during which the animal was not exposed to the linear track, and (iii) "damage", following light-induced hippocampus lesion **(Fig. S1)**. We observed robust single neuron activity across days for up to 8 months **(Fig. 1d-e and Video S1).** We did not notice significant differences between hemispheres and unless stated otherwise, the values reported represent combined data from both hemispheres. Across days, 88 ± 4 % of all neurons in the imaging area were active in each session and 51 ± 17 % were active every session (**Fig. 1f-g and S3**). Within a day, the vast majority of neurons (95 %) were active both while mice explored their home cage or while running in the linear track. However, in the same day between environments (cage or linear track) or across days in the linear track, neurons displayed significant changes in their firing rates (**Fig. S4**). Thus, minimizing motion artifacts using chronic implants and improved signal extraction and registration allowed us to observe that most CA1 neurons that are active one day are also active on subsequent days.

To acquire a comprehensive view of stability of neuronal representations in CA1, we studied both cells that were active in specific locations of the maze when animals were running (defined as "place cells"), and during periods of immobility (defined as "time cells") (*24*, *25*) **(Fig. S5-6)**. Previous work reported that place fields underwent drastic changes across sessions, reaching near random levels (85-75 % change) on the following session (*12*). Under our conditions, we observe that from one day to the next 54 ± 15 % of neurons retained response to a field (defined here as "recurrence", n=56). Surprisingly, despite the initial abrupt change from one day to the next (~46%), the drop in field response for subsequent days was only an additional ~1 % per day, reaching random levels after ~ 50 days (**Fig. 2a-c**). Lastly, these changes in neuronal representations decreased as the animal became more familiar with the task (after the "learning" phase (**Fig. S5**).

Repetitive exposure to the task could induce changes in neuronal representation through continuous updates in place and time fields due to minor changes in environment (i.e. different personnel or odors in the room). To investigate this possibility, we introduced a no-task period in which trained animals were not exposed to the linear track for 10 days. We then compared the changes in place and time cells between animals not exposed to the track and animals which were continuously exposed to the track. Following re-exposure, place and time cells in sessions separated by 11-14 days that included the 10 day period of no-task changed their fields by a similar fraction as animals

bioRxiv preprint doi: https://doi.org/10.1101/559104; this version posted February 24, 2019. The copyright holder for this preprint (which was not certified by peer review) is the author/funder. All rights reserved. No reuse allowed without permission.

continuously exposed to the task in sessions separated by 11 days (**Fig. 2c-d and S7**). Thus, changes in place and time cells happen independently of whether the animal is exposed to the task.

Next, we analyzed whether the fields to which a neuron is responsive changes between sessions. Response fields were relatively similar across days (correlation of 0.7 ± 0.3, n = 505, during the "trained" period between one to 5 days apart) (**Fig. 2f-g**). Interestingly, in some sessions, we observed that 87 ± 8 % of cells changed the direction of their fields by 180 º in the linear track, reversing the directional representation encoded in the previous session (**Fig. 2e**). Rotations of fields happened simultaneously across hemispheres and were accompanied by minimal changes in animal behavior (**Fig. S8**). Similarities of fields across days were significantly lower during periods of learning and during the first two days following re-exposure to the task (**Fig. 2f-g).** During periods of learning or immediately following re-exposure to an environment fields fluctuate, but once the animal becomes familiar with the task, place and time cells can retain their fields even following a 10-day period in which the animal is not exposed to the task.

To investigate whether CA1 representations are also resilient to brain damage we performed local lesions induced by increasing the LED illumination power of the implanted microendoscopes (5 to 10-fold over the threshold needed to visualize GCaMP) (**Fig. 3a**). High illumination intensity induces a local increase in the tissue temperature and affects neurons along a spectrum ranging from perturbing their firing activity to triggering their death. One day after light damage, we observed a massive increase in synchronized firing analogous to interictal discharges (**Fig. 3b**). These abnormal bursts of activity recruited the majority of neurons in the field of view and were direction specific in the linear track **(Fig. S9 and Video S2)**. During days with abnormal CA1 activity, the firing behavior of neurons changed dramatically, and the number of place and time cells increases significantly (**Fig. 3c and S9**). However, during this period, place and time field correlation across days decreased to near random levels **(Fig. 3d-f)**. Interestingly, after 2 to 10 days, abnormal activity ceased overnight and in a similar fashion to what we observed in the re-exposure experiments, after recovery from damage, place and time fields stabilized and a significant portion of place and time cells were responsive to the same fields that they had before the lesion (81 ± 11 % with correlation above 0.7, compared to random $p<10^{-10}$ ranksum, n = 49 sessions) **(Fig. 3f)**.

It has been suggested that groups of neurons with synchronized activity form cell assemblies able to encode learned representations for long periods of time. Cell assemblies encoding temporal and spatial cues have been observed in the hippocampus (*26–28*). However, whether these assemblies develop during learning, how many neurons participate in them, for how many days they persist, and whether they can encode stable information across days is not known. We started analyzing the activity of pairs of neurons, the simplest level of synchronized groups of cells. We observed that neurons in freely moving mice become more synchronized with other neurons within and across hemispheres as mice become familiar with the linear track (**Fig 4a**). This increase in synchrony arises mainly due to the activity of place and time cells. Synchronized pairs of neurons also tended to make the same errors as the animal performed the task, as illustrated in two scenarios. First, whenever one neuron in the pair failed to fire in its field, 50 ± 30 % of the time the other neuron in the pair failed as well. Second, when the pair of neurons fired together, their deviation from the field peak was highly correlated (0.71 ± 0.14, $p<10^{-8}$) (**Fi. 4b**). Across days, we observed that the likelihood of a neuron maintaining its responsiveness to a field on the following day was proportional to the degree of synchrony it had with another neuron in a pair. Altogether, these results support the notion that synchronized activity does not occur simply by chance, and it may be responsible for the stability of representations over time.

To explore this hypothesis, we analyzed correlations of neuronal activity using graph theory to identify whether neuron pairs belong to a larger cell assembly and whether stable information could be encoded in these larger neuronal networks (*26*). Network graphs show a clear behavior-dependent topology, evolving throughout periods of learning and undergoing extensive reorganization upon transition from exploring in the home cage to running in the linear track **(Fig. 4c)**. Graphs revealed the presence of dense clusters comprised of neurons within and across hemispheres whose neurons had preferences for specific behaviors **(Fig. 4d and S10)**. Extraction of these clusters using a Markov diffusion approach identified groups of neurons (defined here as cell groups) encoding direction-specific information about several aspects of the task, including periods of running, immobility, drinking, and turning (**Fig. 4d-f**) (*29*). Synchronized activity of the cell groups were specific for the environment to which the animal was exposed. Cell groups that had synchronous activity in the linear track became asynchronous in the home cage, and vice versa (**Fig. S10**). Individual neurons developed their responsiveness to a field within minutes of exposure to the track. In contrast, cell groups gradually developed their fields over two to four days during the learning phase. Moreover, the task information encoded in these groups did not degrade over time (up to 35 days), even after a 10-day period of no task (**Fig. 4g-i**). Thus, using graph topology we demonstrate that cell groups in CA1 can encode persistent representations of the task across weeks even if the activity of individual neurons varies over time.

The analysis of correlated neuronal activity of CA1 neurons has been used to decode the behavior of the animal or the response of neurons to a field (*30*, *31*), however, it is not known whether this activity can be used to predict whether a cell will be responsive to a field into the future (across days). Using graphs, we observed that the

bioRxiv preprint doi: https://doi.org/10.1101/559104; this version posted February 24, 2019. The copyright holder for this preprint (which was not certified by peer review) is the author/funder. All rights reserved. No reuse allowed without permission.

likelihood that a neuron would maintain its responsiveness to a field over multiple days was proportional to the extent of connectivity in the graph (**Fig. 4j**). To test the hypothesis that graphs can be used to predict the responsiveness of a neuron to a field we analyzed their topology and trained a decoder to determine whether a neuron would be a place or time cell in the future. Using this approach, we show that this synchrony-stability relationship can efficiently decode which neurons in a session will be responsive to a field and predict whether a neuron will maintain its field N sessions apart, even after a period of 10 to 20 days **(Fig. 4k, see methods)**. Furthermore, a decoder trained to identify place and time cells from graph topology in one trained animal in one session can effectively identify place and time cells in other animals simply by analyzing their graph structure (**Fig S11**). Thus, the features of a neuron in a graph are sufficient to decode signatures that are specific to time cells, specific to place cells, or even specific for cells that are neither time or place cells, and these signatures are common between animals.

Discussion

In contrast to previous studies on the stability of CA1 representations, we observed that the vast majority of neurons are active on most days but their firing rate changes across sessions and tasks (*12*). We observe high stability when analyzing the recurrence of place and time cells such that even after 35 days 40 % of neurons were responsive to a field (*12*, *14*). These differences could be due to better registration across days thanks to the use of newer software (CNMFe), a more sensitive CMOS sensor in the microscope, or the use of transgenic animals instead of viral vectors. Our results indicate that hippocampal representations change drastically from one day to the next, but much more slowly thereafter (an additional ~1% change per day), In addition we found that the representations in CA1 were able to recover after an extended period (10 days) without performing the task, or even after abnormal activity induced by local lesions. These manipulations revealed a common feature of information persistence. In both cases, fields undergo transient drifts and fluctuation ultimately converging to a neuronal representation similar to that present before perturbations. This finding provides strong experimental evidence for the presence of attractor-like ensemble dynamics as a mechanism by which the representation of an environment is represented in the hippocampus (*32*). These results suggest a model with two complementary features. First, neuronal representations spontaneously change over time, such that cells whose fields persist longer than 35 days are rare. Second, there are mechanisms that ensure the persistence of representations over short periods of time (days) even if the animals are not training in the task, or if the circuit is perturbed by lesions.

Unlike individual neurons that (on average) only retain information for 10 ± 5 consecutive days, cell groups with synchronous activity encode stable spatial and temporal representation for 35 days (the longest time that we analyzed). Using synchrony to define functional connectivity and graph analysis, we demonstrate that groups of synchronously active neurons provide information absent in individual neurons. The analysis of graph topology had two key benefits. First, the features of a neuron in a graph are sufficient to decode signatures that are characteristic of place cells, time cells or neither, even without having any additional information regarding the animal's behavior. Second, the likelihood that a neuron will maintain its responsiveness to a field in the future is proportional to the extent of connectivity of that neuron in the graph and can be predicted using graph topology. Overall, our findings suggest a model where the patterns of activity of individual neurons gradually change over time while the activity of groups of synchronously active neurons ensures the persistence of representations.

bioRxiv preprint doi: https://doi.org/10.1101/559104; this version posted February 24, 2019. The copyright holder for this preprint (which was not certified by peer review) is the author/funder. All rights reserved. No reuse allowed without permission.

Methods

Animals.

Male and female C57BL6J-Tg-Thy1-GCaMP6s 6 to 20-week old (Jackson Labs stock: 025776) were housed in a reverse 12 h light/dark photocycle and provided food and water ad libitum. Mice were single housed post-surgery until the end of the experiment. Experimental animals were selected randomly and include both sexes. All animal procedures were approved and performed following institutional guidelines (Caltech IACUC).

Bilateral endoscope implantation

Mice were anesthetized with a single dose of 100/10 mg/kg ketamine/xylazine before the surgery and placed into a stereotactic frame and body temperature was maintained with a passive heating pad at 37 ºC. Ketoprofen 5 mg/kg and buprenorphine SR 1 mg/kg was subcutaneously injected prior to surgery. Bupivacaine 1 mg/kg solution added dropwise along the surgical incision prior to wound closure and animals were maintained on ibuprofen 30 mg/mL (in the water) ad libitum for at least 3 days post-surgery. Animals were in a recovery period for at least 4 weeks before attachment of the microendoscope.

Animals underwent unilateral or bilateral surgeries to implant 1.8 mm GRIN lenses directly dorsal to CA1. Before implantation, we performed a 1.8 mm diameter craniotomy centered around the coordinates (relative to bregma: 1.8 mm and -1.8 mm lateral ; -2.0 mm posterior) using a FG1/4 carbide bur. Freshly prepared artificial cerebrospinal fluid (aCSF) was applied to the exposed tissue throughout the surgery to prevent dehydration. Using a blunt 26-gauge needle, the dura, cortex, and portion of the corpus callosum were quickly aspirated under continuous perfusion with aCSF. Aspiration was stopped once a thin layer of horizontal fibers was left on the surface of the hippocampus. The cortical cavity was perfused with more aCSF and small pieces of moist gelfoam were placed on the surface of the craniotomy to prevent excessive bleeding while avoiding contact with the surface of hippocampus. Once the surface of the hippocampus was clear of blood, the GRIN lens was slowly lowered in into the brain using a stereotaxic arm to a depth of 1.30 mm below the surface of the skull. Removal of the cortex and insertion of the GRIN lens was performed in 10 minutes or less (in each hemisphere) to prevent bulging of the hippocampus due to the lower dorsal pressure. Two skull screws were placed anterior to bregma (1.8/-1.8 mm lateral; 1.0 mm anterior) and both the screws and lens were secured with cyanoacrylate and dental cement. The exposed end of the GRIN lens was protected with transparent Kwik-seal glue and animals were returned to a clean cage. Two weeks after the surgery, mice were anesthetized with 1.0 to 2.0 % isoflurane, the glue covering the GRIN lens was removed and a microendoscope was aligned with the GRIN lens. The miniature microscopes were connected to a portable computer which provided live view of the fluorescence image though the endoscopic lens and guided the final alignment and focal plane of the microscope and lens. The microscope was permanently attached to the implant with dental acrylic and the focal sliding mechanism on the microendoscope was sealed with superglue.

Local CA1 damage.

Damage was induced unilaterally by increasing the LED power of the microendoscope to the maximum allowable level. The power of the 470 nm blue LED on the miniscope was measured to produce 500-700 µW at this setting, measured at the end of the GRIN lens facing the CA1 using a power meter (Thorlabs PM100D, S155C probe). The brain was illuminated for at least 30 minutes during the foraging and linear track task. Cell death was quantified as the ratio of neurons active in the field of view prior and after heat damage.

Mouse behavior.

Mice were maintained in a reverse photo cycle and three days prior to initialization of behavior recording they were set under a water restriction protocol in which they receive 2.0 mL of water per day. After three days of water restriction, mice were brought to the recording room and connected to a computer system through a commutator with a 2.0-meter-long custom cable. Animals were habituated to handling and being tethered to the cable for at least 3 days. During this time, mice were connected to the computer and allowed to explore their home cage but were not exposed to the linear track. On the fourth day, behavioral recording was initiated, mice grabbed by the tail and placed in the middle of the track and imaging was recorded within 20 seconds of the mice being introduced in the linear track. Mice were exposed to the maze every day during the learning and first 5 days following re-exposure. However, during the training period or 5 days after re-exposure, recording sessions were at different day intervals ranging from 2-5 days.

Each behavior session consisted of a 10-minute recording of the mouse exploring its home cage without the lid and food dispenser immediately followed (within 30 seconds) by a 20-minute recording of the mouse running on a linear track. The mouse home cage is rectangular 20 cm x 35 cm with 15 cm transparent walls while the linear track is a 1.5-meter-long track 12 cm wide with 15 cm high walls made of white plastic. Three group of cues were place on

bioRxiv preprint doi: https://doi.org/10.1101/559104; this version posted February 24, 2019. The copyright holder for this preprint (which was not certified by peer review) is the author/funder. All rights reserved. No reuse allowed without permission.

both walls of the linear track and consisted of black stripes (2 cm wide) at different angles. The linear track was equipped with an automatic liquid dispensing port that would deliver between 100-200 µL of sugar water (15% sucrose in DI water) at the end of the track. The system would require the animal to run to opposite ends of the track to receive a water reward, a green LED (right side) and red LED (left side) indicated which port was active. A beeping sound was played once mice activated the IR sensor. Delayed reward experiments were performed by decoupling the delivery of sugar reward from IR sensor activation, thus the animal was required to wait for 5 seconds until sugar water was delivered. The beeping sound was not delayed. The position of the mouse was tracked by an ultra-wide-angle webcam at 25 Hz and 640x360 pixels positioned about 1.8 meters above the maze. Mouse position was extracted using OptiMouse (*33*).

Calcium imaging processing.

Video Acquisition: signal from the microendoscope CMOS sensor was acquired thought a UVC compliant USB analog video to digital converter. The video feed was captured and saved by videoLAN media player using custom MATLAB scripts. Data acquisition was set at 25 Hz and display resolution of 720 x 576 pixels using a YUV4:2:2 codec and AVI file encapsulation. All three cameras were synchronized to star simultaneously and were verified to have latencies smaller than 10 ms. Raw videos were offline transcoded to lossless H.264 -MPEG-4 AVC codec and MP4 encapsulation and the first 2 seconds of each video were deleted. Transcoded videos were filtered using a high quality 3-dimensional low pass filter (*hqdn3d*) with spatial and temporal smoothing of 4x4 pixels and 2 frames, respectively. Denoised videos were then 4x down-sampled by a moving window averaging of 4 frames. All transcoding, smoothing, and down sampling was performed by the open source program ffmpeg controlled through custom MATLAB scripts. Down sampled videos were motion corrected using the recursive fast Fourier transform approach provided in the MATLAB script *sbxalign.mat* from Scanbox. For batch analysis all 4x down-sampled videos were concatenated into a larger video, motion corrected, and analyzed with CNMFe.

Signal extraction: motion corrected videos were saved as a matrix array and analyzed using CNMFe with a 2-fold spatial and temporal down-sampling (*22*, *23*). All 7450 frames of calcium imaging during the 20-minute linear track task or 3750 frames during home cage exploration were analyzed simultaneously. In some cases, were motion artifacts were minimal, up to 200,000 frames of data was analyzed simultaneously with CNMFe and these datasets were utilized to confirm registration procedures described below. All data analysis was performed using the deconvoluted neural activity output (neuron.S) from CNMFe.

Cell registration: accurate alignment of neurons across sessions spanning days to months has noticeably become a challenging aspect of calcium imaging. Taking from studies using multiphoton imaging, registration approaches using single photon epifluorescence involves alignment of neurons between sessions based on their spatial footprint. However, spatial footprint of extracted neurons using microendoscopes can suffer from artifacts arising from changes in firing rates, extraction algorithms, and motion correction artifacts. These effects are compounded when imaging areas with dense labeling as observed in transgenic animals. To overcome these limitations, we employed an interleaved and batch data analysis approach in which a session of data was common between two days to be aligned. This common session served the purpose of decrease noise in the extracted neuron footprints and provided firing data common to both datasets. First, the footprint extracted by CNMFe was thresholder so that only the pixels above the 50th percentile formed the ROI footprint. Minor motion artifacts were corrected by a fast Fourier transform method using the PNR image output from CNMFe. The spatial correlation between all neurons with centroid distances below 15 pixels between the two alignment datasets was calculated. The correlation of the CNMFe deconvoluted neural activity was also calculated for all neuron pairs with centroid distance less than 15 pixels. Only spatial and temporal correlation above 0.5 and 0.3, respectively, were considered. An alignment coefficient was calculated by multiplying the spatial correlation and temporal correlation of every potential neuron pair. The alignment coefficient was binned in 100 intervals and the probability distribution calculated. A plot of the probability distribution showed a clear bimodal distribution **(Fig. S2f)**, a threshold of approximately 0.5 was selected manually. All neuron pairs below this threshold were deleted, and the remaining were aligned based on a iterative selection of pairs with the highest alignment coefficient. This approach was validated by aligning a video to itself, where we observed that including temporal information increased aligning accuracy by about 10% (see supplementary information). Here, we take advantage of small motion artifacts across days in order to motion correct and analyze several days together in one animal. This ensures, that even if the neuron decreases is firing rate significantly, CNMFe will still draw a ROI around the neuron and extract its firing activity.

Data analysis

bioRxiv preprint doi: https://doi.org/10.1101/559104; this version posted February 24, 2019. The copyright holder for this preprint (which was not certified by peer review) is the author/funder. All rights reserved. No reuse allowed without permission.

Identifying place cells: place fields were extracted by identifying periods when mice ran continuously faster than 3 cm/second for more than 0.4 seconds. Together, these thresholds eliminate periods during which mice were grooming, rearing, or turning. The length of the linear track was divided into bins spanning 3 centimeters (50 bins), neuronal activity at the ends of the maze (7 cm) were not included in the analysis. The average firing rate of a neuron in each bin was calculated by the sum of all calcium activity in a bin divided by the amount of time the mouse spent in that bin. The average firing rate of a neuron was then normalized by the total number of spikes in order to generate normalized tuning profile of each neuron. Neurons were classified as place cells if: (1) the place field is 15 cm wide; (2) calcium transients were present > 30 % of the time the mouse spent in the place field; and (3) the cell contains significantly greater spatial information than chance. Spatial information is calculated using (*34*):

$$SI = \frac{1}{\lambda}\sum_i \lambda_i \log_2\left(\frac{\lambda_i}{\lambda}\right) P_i$$

where λ is the overall average calcium transient rate of the cell, λ_i is the average calcium transient rate in spatial bin *i* and P_i is the probability the mouse is in spatial bin *i*. Chance level spatial information for each neuron is calculated by shuffling the time stamps of the calcium transients and calculating the spatial information of the shuffled trace. This is done for 1000 iterations and the spatial information of the cell is considered significant if it is higher than 95% of the shuffled traces.

Identifying time cells: the linear track was equipped with a LED light that would turn off once the animal activated the IR sensors near the water reward port. The ON/OFF transition of the LED in the behavior video was extracted and used as a timestamp. The LED timestamp was set as time = 0 and a window of 31 frames or the time the animal was immobile (velocity less 1 cm/sec), whichever is smaller, was used for analysis. Neurons were classified as time cells if: (1) they fire at least 20% of the times the animal activated the water port; (2) the neuron fired 30% more within its field (20 % of time immobile); and (3) the cells contain significantly greater information than chance. Temporal information was calculated using the same equation above but using λ as the average activity during immobility, λ_i is the average activity in frame *i* after activation of the water port. The variable Pi in this case represent the probability that the animal was not moving during frame *i*.

Network graphs: an adjacency matrix was generated by calculating the pairwise Pearson correlation between all neurons during a session. Only statistically significant ($p<0.05$) correlation values above 0.10 were used to build the adjacency matrix. The weight of the edge between two neurons was set to be equal to the correlation coefficient. The networks are plotted with the network graphical tool (Gephi 0.9.2, www.gephi.com) using the built-in ForceAtlas2 layout. Modularity was calculated with Markov Diffusion approach with a diffusion time of one using MATLAB scrips as previously described (*29*). Cell groups are defined as cells making up each module extracted by the modularity calculation. Only the largest 11 modules were analyzed. The degree, average clustering coefficient, eigenvector centrality, and PageRank were calculated using built in and custom MATLAB functions.

Behavior decoding: mouse position was decoded by a generalized linear model using the *glmfit* function with a normal distribution in MATLAB. Mouse position was discretized into 50 intervals and periods of mobility and immobility were decoded. The linear model was first trained with 50% of randomly selected place/time cell activity and mouse position and then tested on the remaining 50%. For time-lapse decoding we used the decoder trained in one session (M) to decode the position M+N sessions apart using the activity of the same place/time cells on day N. Decoding mouse position using cell groups was performed in a similar fashion, but instead of using place/time cell activity we used the integrated deconvoluted neuronal activity of neurons making up each cell group. Thus, we had 11 inputs (for each cell group) and one target (mouse position) as a training set, 70 % of the dataset was used for training. Time-lapse decoding was performed by training a decoder on one sessions and then testing it on session N using cell group activity as an input. Cell group activity was determined at sessions N by first calculating the maximum projection of the adjacency matrix across 5 trained sessions (5-10), calculating the cell groups using Markov diffusion. The IDs of neurons making each cell group were use to calculate their integrated group activity in all other session. In addition, to account for the nonlinear and asymmetric nature of fields encoded by cell groups, we also performed position decoding using a nonlinear fitting neural network (*fitnet* function in MATLAB). This network was set to have 50 hidden layers and trained with 70% of randomized cell group activity and mouse position, validated with 15 % and tested with 15%. The network trained in one session was used to decode N sessions apart. In all, cases we also trained the decoders with a randomized dataset for comparison. Error reported represent the median ± sem across N sessions apart including periods of learning and no task.

Time/place cell decoding: whether a neuron was place/time cell was decoded from neuronal activity by (1) calculating the intrahemispheric correlation in one session, (2) generating a graph and calculating its topological properties, (3) training a fitting neural network with half the data, (4) use the decoder trained on one session to decode another session. Graph topology metrics for each node included: degree, modularity, eigenvector centrality, PageRank, calcium activity, and the assemblies to which a node was connected. The calcium activity was defined as the integrated

bioRxiv preprint doi: https://doi.org/10.1101/559104; this version posted February 24, 2019. The copyright holder for this preprint (which was not certified by peer review) is the author/funder. All rights reserved. No reuse allowed without permission.

intensity of a neuron in a session minus the median integrated intensity of all neurons. All metric, excluding modularity, calcium activity, and node connectivity were normalized so that the sum in a session is equal to one. These metrics were the input to the neural network decoder and whether a neuron had (1) or not (0) a field was used as the training target. In addition, we trained a decoder simultaneously with 10 sessions of data from one mouse and used to decode which neurons were place and time cells in other animals only using their graph topology.

Decoding stability of a cell: we predicted whether a place/time cell observe today will lose its field in N days by first randomly selecting 50 % of the sessions in one mouse and calculating all pairwise session intervals between them. We trained one fitting neural network for each set of sessions separated at a N interval, generating N decoders. The inputs consisted of graph topology metrics calculated from brain activity (the same parameters used above) recorded in the sessions at N intervals. The target dataset was a matrix listing whether a neuron became responsive or unresponsive to a field (logical 1) or the neuron retained its field or lack thereof (logical 0) between two sessions at a N interval. We then tested each decoder on the remaining 50 % of the sessions with intervals ranging from 1 to N. We filtered the decoder's output so that the highest outputs above the median were considered positive.

bioRxiv preprint doi: https://doi.org/10.1101/559104; this version posted February 24, 2019. The copyright holder for this preprint (which was not certified by peer review) is the author/funder. All rights reserved. No reuse allowed without permission.

References

1. W. B. Scoville, B. Milner, Loss of Recent Memory After Bilateral Hippocampal Lesions. *Journal of Neurology, Neurosurgery & Psychiatry*. **20**, 11–21 (1957).

2. N. J. Cohen, L. R. Squire, Preserved learning and retention of pattern-analyzing skill in amnesia: dissociation of knowing how and knowing that. *Science*. **210**, 207–210 (1980).

3. J. O'Keefe, J. Dostrovsky, The hippocampus as a spatial map. Preliminary evidence from unit activity in the freely-moving rat. *Brain Research*. **34**, 171–175 (1971).

4. A. Czurkó, H. Hirase, J. Csicsvari, G. Buzsáki, Sustained activation of hippocampal pyramidal cells by 'space clamping' in a running wheel. *European Journal of Neuroscience*. **11**, 344–352 (1999).

5. D. Aronov, R. Nevers, D. W. Tank, Mapping of a non-spatial dimension by the hippocampal–entorhinal circuit. *Nature*. **543**, 719–722 (2017).

6. M. R. Mehta, C. A. Barnes, B. L. McNaughton, Experience-dependent, asymmetric expansion of hippocampal place fields. *Proceedings of the National Academy of Sciences*. **94**, 8918–8921 (1997).

7. M. A. Wilson, B. L. McNaughton, Dynamics of the hippocampal ensemble code for space. *Science*. **261**, 1055–1058 (1993).

8. N. T. Agnihotri, R. D. Hawkins, E. R. Kandel, C. Kentros, The long-term stability of new hippocampal place fields requires new protein synthesis. *Proceedings of the National Academy of Sciences*. **101**, 3656–3661 (2004).

9. C. G. Kentros, N. T. Agnihotri, S. Streater, R. D. Hawkins, E. R. Kandel, Increased Attention to Spatial Context Increases Both Place Field Stability and Spatial Memory. *Neuron*. **42**, 283–295 (2004).

10. J. Debiec, J. E. LeDoux, K. Nader, Cellular and Systems Reconsolidation in the Hippocampus. *Neuron*. **36**, 527–538 (2002).

11. L. T. Thompson, P. J. Best, Long-term stability of the place-field activity of single units recorded from the dorsal hippocampus of freely behaving rats. *Brain Research*. **509**, 299–308 (1990).

12. Y. Ziv *et al.*, Long-term dynamics of CA1 hippocampal place codes. *Nature Neuroscience*. **16**, 264 (2013).

13. J. D. Zaremba *et al.*, Impaired hippocampal place cell dynamics in a mouse model of the 22q11.2 deletion. *Nature Neuroscience*. **20**, 1612–1623 (2017).

14. T. Hainmueller, M. Bartos, Parallel emergence of stable and dynamic memory engrams in the hippocampus. *Nature*, 1 (2018).

15. N. B. Danielson *et al.*, Sublayer-Specific Coding Dynamics during Spatial Navigation and Learning in Hippocampal Area CA1. *Neuron*. **91**, 652–665 (2016).

16. S. M. Zola-Morgan, L. R. Squire, The primate hippocampal formation: evidence for a time-limited role in memory storage. *Science*. **250**, 288–290 (1990).

17. H. A. Zariwala *et al.*, A Cre-Dependent GCaMP3 Reporter Mouse for Neuronal Imaging In Vivo. *J. Neurosci.* **32**, 3131–3141 (2012).

18. D. J. Cai *et al.*, A shared neural ensemble links distinct contextual memories encoded close in time. *Nature*. **534**, 115–118 (2016).

bioRxiv preprint doi: https://doi.org/10.1101/559104; this version posted February 24, 2019. The copyright holder for this preprint (which was not certified by peer review) is the author/funder. All rights reserved. No reuse allowed without permission.

19. H. Dana *et al.*, Thy1-GCaMP6 transgenic mice for neuronal population imaging in vivo. *PLoS ONE*. **9**, e108697 (2014).

20. K. K. Ghosh *et al.*, Miniaturized integration of a fluorescence microscope. *Nature Methods*. **8**, 871 (2011).

21. W. A. Liberti, L. N. Perkins, D. P. Leman, T. J. Gardner, An open source, wireless capable miniature microscope system. *J. Neural Eng.* **14**, 045001 (2017).

22. E. A. Pnevmatikakis *et al.*, Simultaneous Denoising, Deconvolution, and Demixing of Calcium Imaging Data. *Neuron*. **89**, 285–299 (2016).

23. P. Zhou *et al.*, Efficient and accurate extraction of in vivo calcium signals from microendoscopic video data. *eLife*. **7**, doi:10.7554/eLife.28728.

24. C. J. MacDonald, K. Q. Lepage, U. T. Eden, H. Eichenbaum, Hippocampal "Time Cells" Bridge the Gap in Memory for Discontiguous Events. *Neuron*. **71**, 737–749 (2011).

25. K. Kay *et al.*, A hippocampal network for spatial coding during immobility and sleep. *Nature*. **531**, 185 (2016).

26. K. D. Harris, J. Csicsvari, H. Hirase, G. Dragoi, G. Buzsáki, Organization of cell assemblies in the hippocampus. *Nature*. **424**, 552 (2003).

27. V. Itskov, C. Curto, E. Pastalkova, G. Buzsáki, Cell Assembly Sequences Arising from Spike Threshold Adaptation Keep Track of Time in the Hippocampus. *J. Neurosci.* **31**, 2828–2834 (2011).

28. E. Pastalkova, V. Itskov, A. Amarasingham, G. Buzsáki, Internally Generated Cell Assembly Sequences in the Rat Hippocampus. *Science*. **321**, 1322–1327 (2008).

29. Y. N. Billeh, M. T. Schaub, C. A. Anastassiou, M. Barahona, C. Koch, Revealing cell assemblies at multiple levels of granularity. *Journal of Neuroscience Methods*. **236**, 92–106 (2014).

30. R. J. Low, S. Lewallen, D. Aronov, R. Nevers, D. W. Tank, Probing variability in a cognitive map using manifold inference from neural dynamics. *bioRxiv*, 418939 (2018).

31. L. Meshulam, J. L. Gauthier, C. D. Brody, D. W. Tank, W. Bialek, Collective Behavior of Place and Non-place Neurons in the Hippocampal Network. *Neuron*. **96**, 1178-1191.e4 (2017).

32. A. Samsonovich, B. L. McNaughton, Path Integration and Cognitive Mapping in a Continuous Attractor Neural Network Model. *J. Neurosci.* **17**, 5900–5920 (1997).

33. Y. Ben-Shaul, OptiMouse: a comprehensive open source program for reliable detection and analysis of mouse body and nose positions. *BMC Biology*. **15**, 41 (2017).

34. W. E. Skaggs, B. L. McNaughton, K. M. Gothard, in *Advances in Neural Information Processing Systems 5*, S. J. Hanson, J. D. Cowan, C. L. Giles, Eds. (Morgan-Kaufmann, 1993; http://papers.nips.cc/paper/671-an-information-theoretic-approach-to-deciphering-the-hippocampal-code.pdf), pp. 1030–1037.

bioRxiv preprint doi: https://doi.org/10.1101/559104; this version posted February 24, 2019. The copyright holder for this preprint (which was not certified by peer review) is the author/funder. All rights reserved. No reuse allowed without permission.

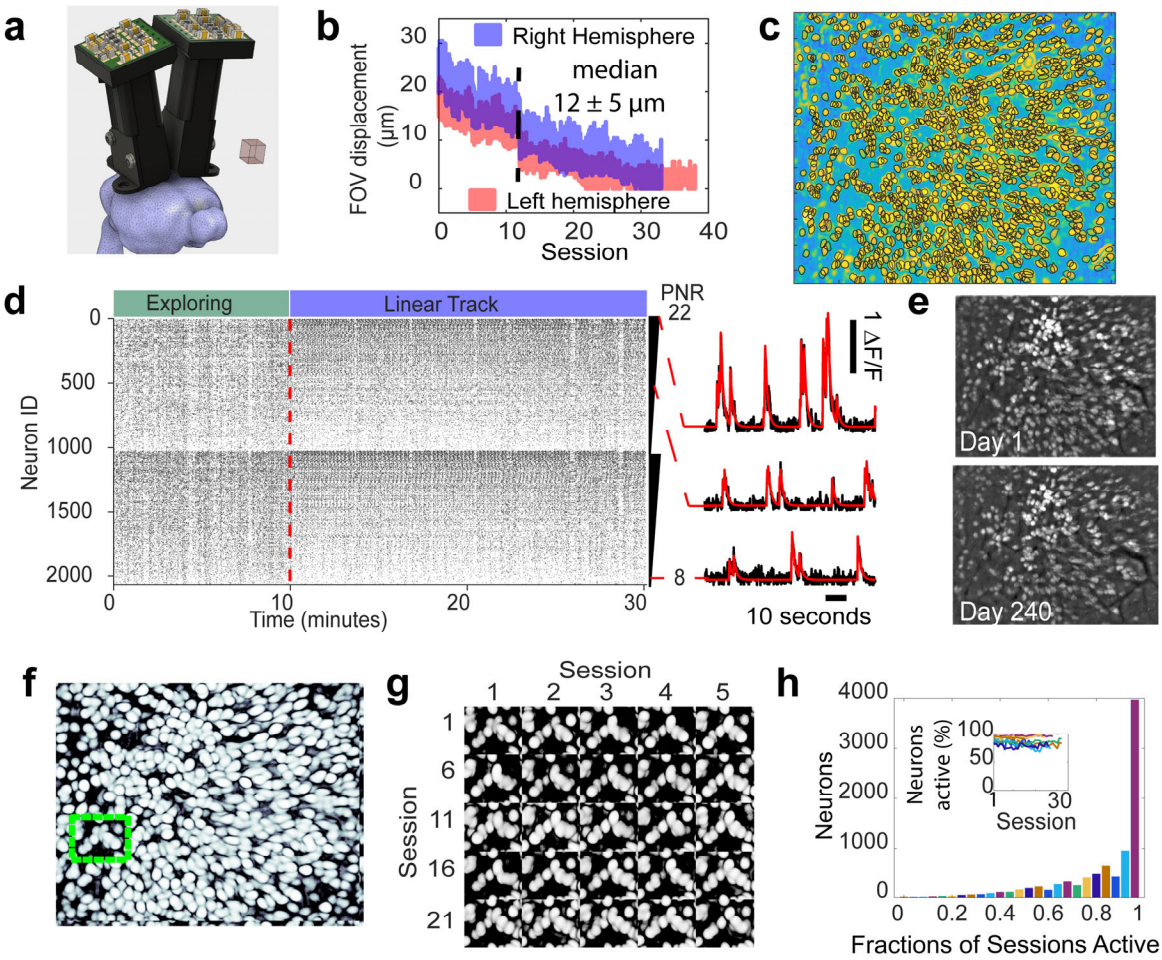

Figure 1. **Long-term simultaneous bilateral imaging of CA1 activity in freely moving transgenic mice**. **(a)** Rendering of custom endoscope used in the bilateral configuration. **(b)** Chronic implants show small field of view (FOV) displacement across weeks. Dashed line represents period of no task (10 days). **(c)** Multiple sessions (25) combined and analyzed simultaneously using CNMFe (see methods). **(d)** Raster plot of deconvoluted neuronal activity in the right (top) and left (bottom) hemisphere of a trained freely moving mouse. Neurons are ranked from high to low peak-to-noise ratio (PNR). Between 754-1480 neurons were recorded per hemisphere, median 1236, in 4 bilateral mice and 5 with unilateral microendoscopes). (**e**) Maximum intensity projection in the field of view in one animal recorded for 8 months. (**f-g**) Intensity correlation map of a single session (*left*) and a small region of interest (green rectangle) showing the persistence of activity throughout 25 sessions (*right*). (**h**) Activity distribution of the right hemisphere showing that the majority of neurons are active on most sessions (n=8 mice).

bioRxiv preprint doi: https://doi.org/10.1101/559104; this version posted February 24, 2019. The copyright holder for this preprint (which was not certified by peer review) is the author/funder. All rights reserved. No reuse allowed without permission.

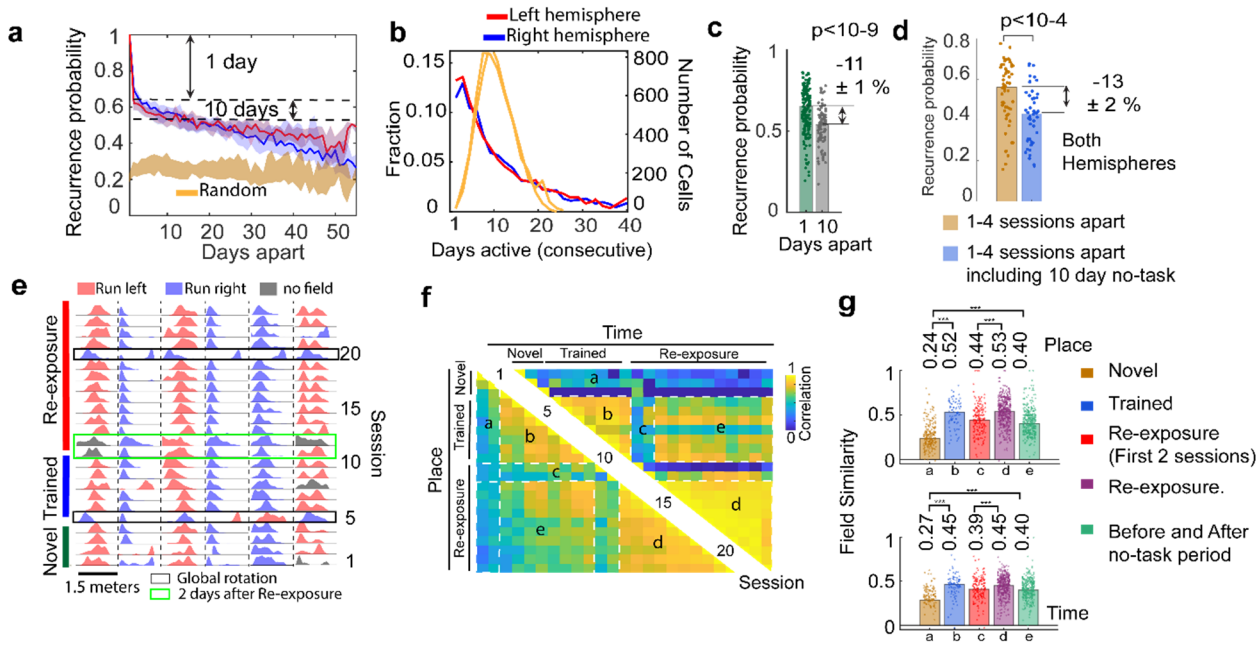

Figure 2. **Spatial and temporal representations persist through periods of no exposure to the task**. **(a)** The probability of a neuron with place and time field in one session having any place/time information N days apart. Solid lines represent the median and shadow the 95 % bootstrap confidence interval. Random level represent overlap if neurons randomly became responsive to a field on the following day. **(b)** Distribution of neurons retaining their field response for N consecutive sessions. **(c)** Quantification of cell overlap 1 day apart (65 ± 14 %, n = 193 sessions) and 10 days (54 ± 12 %, n = 97, ranksum-test) when continuously exposed to the track. **(c)** Quantification of cell overlap 1-4 sessions apart (65 ± 14 %, n = 193 sessions) and 1-4 sessions days (54 ± 12 %, n = 97, ranksum-test) when including a 10-day period of no task. **(e)** Response fields of six place cells across 45 days. Black rectangles show sessions in which 87 ± 8 % of fields changed direction. Green rectangle are the two sessions after re-exposure. **(f)** Pair-wise field correlation of neurons in the right hemisphere with a field response between sessions. Colors represent the median value. Numbers indicate the session. Sessions were grouped as indicated by the dashed rectangle and letters. **(g)** The similarity between fields in each group of sessions was obtained by subtracting the correlation obtained by random aligning neurons (n = 7, right hemisphere, each dot is the median between two sessions, $p < 10^{-4}$ marked by ***).

bioRxiv preprint doi: https://doi.org/10.1101/559104; this version posted February 24, 2019. The copyright holder for this preprint (which was not certified by peer review) is the author/funder. All rights reserved. No reuse allowed without permission.

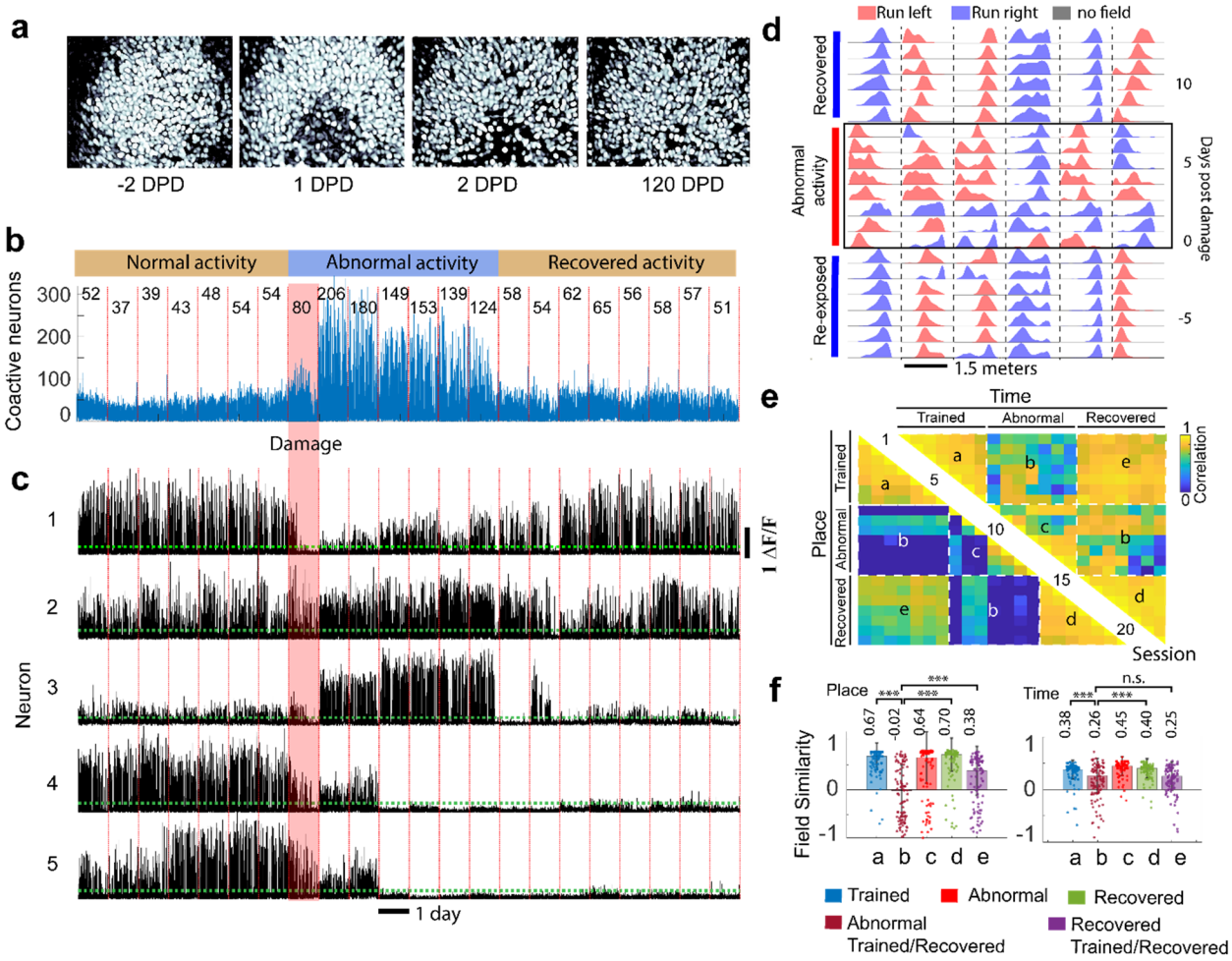

Figure 3. Tissue heating induces direction specific bursting activity and unstable fields followed by partial recovery of the original representation. (a) Intensity correlation of a 20-minute session before, during, and after tissue damage induced by high illumination intensity (DPD, days post damage). **(b)** Number of neurons active simultaneously (within 160 milliseconds) during each session (number shows median of the largest 90% bursts). Each day is marked by a vertical red line. **(c)** Single neuron activity across days while the mouse runs in the linear track (black traces) showing changes in activity induced by tissue damage (red rectangle). The horizontal green line shows the 3 standard deviation of the background fluctuations. Top two neurons recover from the damage, middle neuron is highly active during abnormal activity, and the last two neurons become inactive following damage. **(d)** Activity distribution of six place cells showing the high instability of fields during abnormal activity, colors as in figure 2. Black rectangle shows sessions with abnormal activity. **(e)** Pair-wise correlation between sessions of neurons which retained their fields (right hemisphere). (f) The similarity between fields in groups of sessions before, during, and after the lesion (n = 2 mice, each dot is median of session pair, numbers are median, p< 10-4 marked by ***).

bioRxiv preprint doi: https://doi.org/10.1101/559104; this version posted February 24, 2019. The copyright holder for this preprint (which was not certified by peer review) is the author/funder. All rights reserved. No reuse allowed without permission.

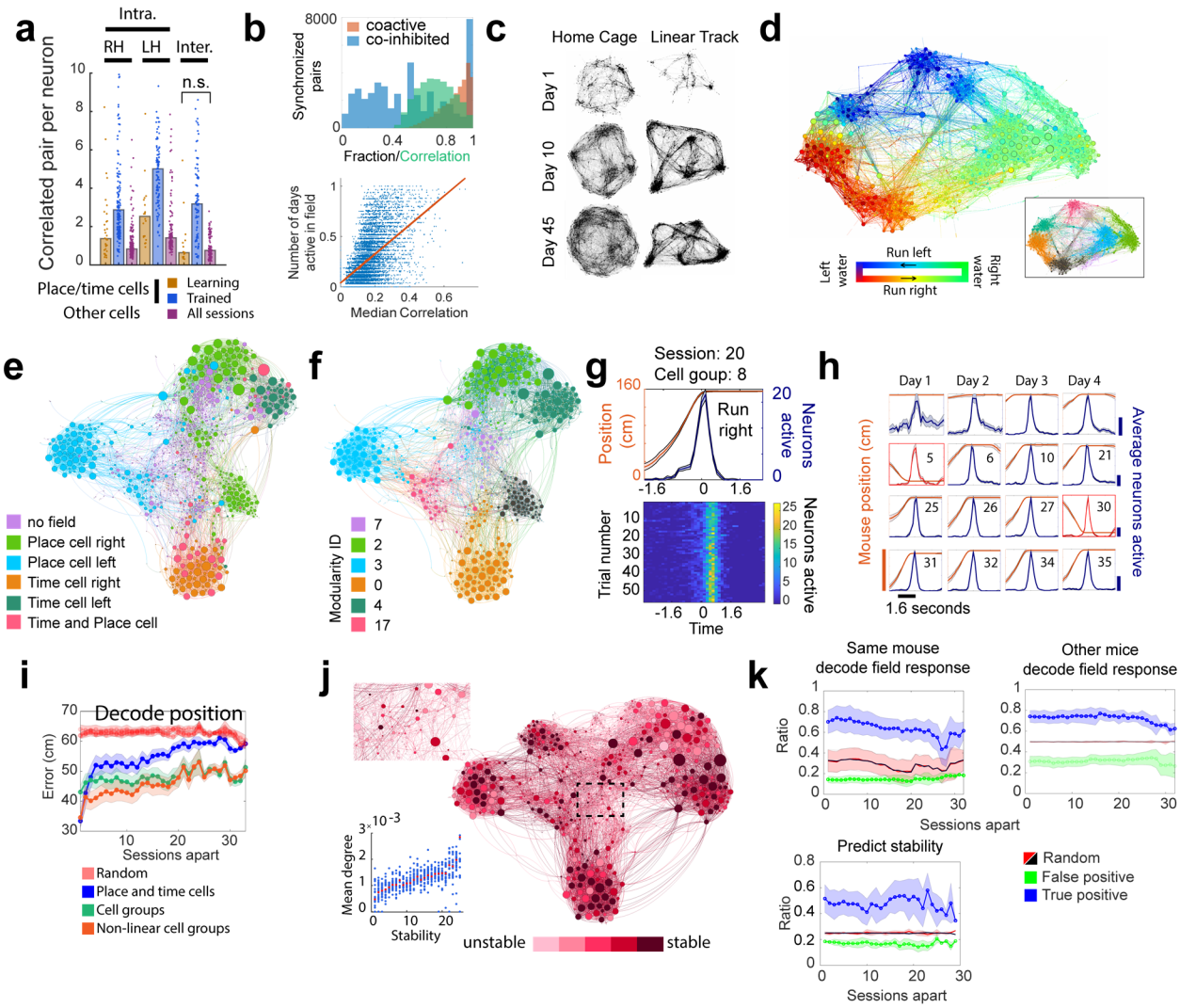

Figure 4. Synchronous activity in group of cells encode stable representations of the task. (a) number of inter- and intra-hemispheric synchronous pairs as a function of training (4 mice, each dot represents a session in one mouse, all significant $p<10^{-6}$). **(b)** (Top) Neuron pairs are co-active 90 ± 3 % (orange distribution) of the time and fail to fire synchronously 50 ± 20 % of the time (blue distribution). Synchronized pairs also show correlated fluctuations of their fields (green distribution, 0.77 ± 0.17, $p<10^{-8}$). (Bottom) The number of sessions they remain responsive a field is proportional to the level of synchrony in the pair (R-square 0.35, $p< 10^{-4}$). **(c)** Graph topology in the linear track and home cage of one mouse during learning, trained, and re-exposed periods (data from one hemisphere used, lines represent correlation > 0.15, neurons shown as nodes). **(d)** Graph colored by the median location where each neuron (node) was active during a 20 minute session in the linear track. Inset shows the same graph but colored by cell groups (see methods, right hemisphere). Graph of neuronal activity in the linear track colored by **(e)** experimentally determined field responses and **(f)** by the largest six cell groups identified by Markov diffusion. The size of each node corresponds to the degree (number of connecting lines) of each node. **(g)** (Top panel) Integrated activity of neurons in a cell group during a linear track session and (bottom panel) activity each time the mouse ran through the cell group's receptive field. **(h)** Persistence of a cell group identified by neuronal activity from days 5-6 (shadows represent deviation during a session). **(i)** Mouse position in the linear track decoded using all place/time cells (132 to 639 neurons, errors 10-19 cm using generalized model), or the summed activity of all neurons in 11 cell groups (error 13-17 using a generalized model or a 12-15 nonlinear fitting neural network). The performance of decoders using cell group activity outperformed place/time cell decoders on long-timescales (20+ sessions apart, random vs place/time decoder p=0.210 and random vs cell group decoder, $p<10^{-5}$, Friedman-test). **(i)** Activity of one cell group across 35 days (number indicate day, red traces indicate sessions with rotated representations). **(j)** Graph colored by the fraction of sessions a neuron was classified as time or place cell, larger nodes have larger number of synchronous pairs. Top

bioRxiv preprint doi: https://doi.org/10.1101/559104; this version posted February 24, 2019. The copyright holder for this preprint (which was not certified by peer review) is the author/funder. All rights reserved. No reuse allowed without permission.

inset shows the presence of unstable nodes with low connectivity, bottom inset shows quantification of degree and stability across 25 sessions (red dots mark median, R-square XX). **(k)** A decoder trained with graph topology metrics on one day can identify 71 ± 11 % of all place/time cells the next day and 59 ± 10 % after 30 days in the same mouse (left) with similar results obtained when a decoder trained with one mouse is used to identify place/time cells in other mice (n = 7, right). It also identifies 86 ± 2 % of neurons with no field responses. (Right) Neurons which will become responsive or unresponsive to a field between two re-exposures to the track N sessions apart can be decoded from graph metrics 46 ± 5 % of the time.